Journal of Solid State Chemistry 184 (2011) 818–824

Contents lists available at ScienceDirect

Journal of Solid State Chemistry

journal homepage: www.elsevier.com/locate/jssc

Synthesis and characterization of hybrid materials based on 1-butyl-3-methylimidazolium tetrafluoroborate ionic liquid and Dawson-type tungstophosphate $K_7[H_4PW_{18}O_{62}]\cdot 18H_2O$ and $K_6[P_2W_{18}O_{62}]\cdot 13H_2O$

Malika Ammam*, Jan Fransaer

Department of Metallurgy and Materials Engineering (MTM), K.U Leuven, Kasteelpark Arenberg 44, B-3001 Heverlee, Belgium

ARTICLE INFO

Article history:
Received 26 July 2010
Received in revised form
26 January 2011
Accepted 6 February 2011
Available online 15 February 2011

Keywords:
Well-Dawson polyoxometalates
Room temperature ionic liquid
Hybrid material ionic liquid-polyoxometalates

ABSTRACT

In this study, we synthesized hybrid materials using well-Dawson polyoxometalates (POMs), $K_7[H_4PW_{18}O_{62}]\cdot 18H_2O$ or $K_6[P_2W_{18}O_{62}]\cdot 13H_2O$ and a room temperature ionic liquid 1-butyl-3-methylimidazolium tetrafluoroborate ([BMIM][BF_4]). K, W, P and CHN elemental analysis showed that one mole of $[H_4PW_{18}O_{62}]^{7-}$ reacts with 6 moles of $BMIM^+$ and one mole of $[P_2W_{18}O_{62}]^{6-}$ reacts with 4 moles of $BMIM^+$ to form, respectively, $K[BMIM]_6H_4PW_{18}O_{62}$ and $K_2[BMIM]_4P_2W_{18}O_{62}$. X-ray diffraction illustrated amorphous structure of the hybrid materials. FT-IR spectra showed the presence of both 1-butyl-3-methylimidazolium cation and the Dawson anion. TG analysis displayed a relative thermal stability of the hybrid materials compared to the parents Dawson POMs. Cyclic voltammetry showed that the reduction peak potentials of the Dawson anion in the hybrid materials shift towards negative values and the shift is more pronounced for $K[BMIM]_6H_4PW_{18}O_{62}$ compared to $K_2[BMIM]_4P_2W_{18}O_{62}$. This was attributed to a decrease in the acidity of the Dawson POM anion in the hybrid material.

1. Introduction

Polyoxometalates (POMs), as early transition-metal clusters, attract extensive interest in fields such as catalysis, ion exchange, electrochemistry, electrochromism, magnetism, and in medicine [1–7]. The synthesis and development of hybrid organic–inorganic nanocomposites based POMs have emerged as one of the most potentially significant fields of investigation in contemporary materials chemistry [8–20]. Such hybrid materials are widely regarded as offering the key to overcome challenges in areas such as photochromism [10,16,17], catalysis [14,15], and as fast proton conductors [18,21–23]. The pairing of POM anions with organic cations and ionic liquids (ILs) continue to yield interesting materials, including a recent report on the synthesis of ambient temperature POM based ionic liquids [24]. Inorganic POMs are solid materials having a boosted acidity and these metal oxide framework anions can react with room temperature ionic liquids to yield new organic–inorganic hybrid composite materials [19,20,23]. For POMs based Keggin $[XM_{12}O_{40}]^{n-}$, where X is the heteroatom (P^V or Si^{IV}), M is the addenda atom (Mo^{VI} or W^{VI}), and O represents oxygen, the structure of the POM anion maybe retained in the hybrid material showing hybrid properties of both Keggin anion and the organic part [19,20]. Synthesis of new hybrid materials based POMs and ILs is important to understand the nature of interactions between the POM anion and organic cations and their stability in the molecular material [25]. More importantly, the purpose is to explore their potential applications.

Recently, research in our laboratory [26] has shown that the deposition of the hybrid materials based on Keggin POMs and ILs, 1-butyl-3-methylimidazolium-silicotungstic acid and 1-butyl-3-methylimidazolium-phosphomolybdic acid salts on stainless steel electrodes exhibit a capacitor behavior. For example, in media of 0.5 M Na_2SO_4 (pH 7), the hybrid material 1-butyl-3-methylimidazolium-silicotungstic acid/stainless steel electrode has a stable specific capacitance close to 172 Fg^{-1}. This result prompted us to extend our investigation to other families of POMs. In the course of this work, we have investigated the pairing of well-Dawson POMs, the dissymmetrical-type $K_7[H_4PW_{18}O_{62}]\cdot 18H_2O$ and the symmetrical-type $K_6[P_2W_{18}O_{62}]\cdot 13H_2O$ with 1-butyl-3-methylimidazolium cations. The synthesized hybrid materials were characterized by K, P, W and CNH analysis, SEM, XRD, FT-IR, TG analysis and cyclic voltammetry.

2. Experimental

2.1. Chemicals

Ultrapure water milliQ grade with a resistance of 18.2 MΩ cm was used for all experiments. Well-Dawson POMs, $K_7[H_4PW_{18}O_{62}]\cdot 18H_2O$ (abbreviated as PW_{18}) and $K_6[P_2W_{18}O_{62}]\cdot 13H_2O$ (abbreviated as

* Corresponding author. Fax: +32 16 321991
E-mail address: m78ammam@yahoo.fr (M. Ammam).

0022-4596/$ - see front matter © 2011 Elsevier Inc. All rights reserved.
doi:10.1016/j.jssc.2011.02.002

P_2W_{18}) were synthesized and characterized according to the procedure reported by Contant et al. [27] and Contant [28]. 1-butyl-3-methylimidazolium tetrafluoroborate ([BMIM][BF_4]) was obtained from IoLiTec. Dimethylsufoxide (DMSO) and $NaClO_4$ from Acros Organic. K_2HPO_4 and $NaWO_4$ from Sigma-Aldrich. Glassy carbon rod (1 mm diameter) was purchased from Alfa Aesar.

2.2. Synthesis of the hybrid materials

The synthesis of 1-butyl-3-methylimidazolium-PW_{18} and 1-butyl-3-methylimidazolium-P_2W_{18} salts is carried out by taking, respectively, 11:1 and 6:1 mole ratio in order to prepare 1 mole of each hybrid salt assuming that all the K^+ and protons in the Dawson units will be replaced by $BMIM^+$. More precisely, 4.93 g of PW_{18} was dissolved in ultrapure water and under constant stirring 2.48 g of [BMIM][BF_4] was added to the solution. A white precipitate is formed immediately upon addition of the first drop of the ionic liquid to the POM solution. The white precipitate was filtered off and washed several times with ultrapure water and oven dried at 60 °C. CHN Anal. calcd. (found): C: 18.01(11.41), H: 2.82(2.21), N: 5.25(3.23). Anal. (Found): K: (0.72), W: (63.73) and, P: (0.61).

Similarly, for the synthesis of 1-butyl-3-methylimidazolium-P_2W_{18}, 4.83 g of P_2W_{18} was dissolved in ultrapure water and under constant stirring 1.35 g of [BMIM][BF_4] was added to the solution and a white–yellow precipitate is formed. The precipitate was filtered off and washed several times with ultrapure water and oven dried at 60 °C. CHN Anal. calcd. (found): C: 11.07(7.71), H: 1.73(1.78), N: 3.23(2.37). Anal. (Found): K: (1.51), W: (66.02) and, P: (1.21). Fig. 1 shows the structure of the room temperature ionic liquid ([BMIM][BF_4]) (Fig. 1A), structure of the well-Dawson dissymmetrical-type PW_{18} (Fig. 1B), and well-Dawson symmetrical-type P_2W_{18} (Fig. 1C).

2.3. Equipment and methodology

The hybrid materials were analyzed by CHN elemental analyzer CE Instruments EA-1110. Inductively Coupled Plasma Emission Spectrometer (ICP-OES) from Varain model Vista-MPX was used to estimate the K, P and W content in the hybrid materials.

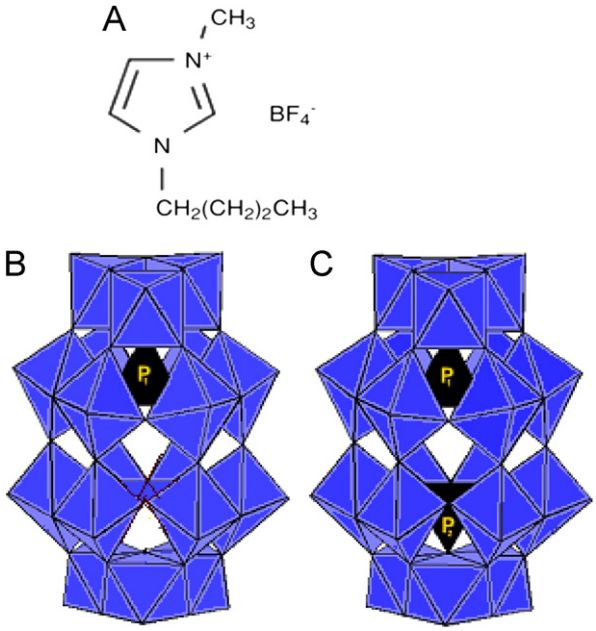

Fig. 1. (A) Structure of the room temperature ionic liquid 1-butyl-3-methylimidazolium tetrafluoroborate, (B) structure of the well-Dawson dissymmetrical-type PW_{18}, and (C) structure of the well-Dawson symmetrical-type P_2W_{18}.

Scanning electron microscopy (SEM) was carried out using JEOL JSM 6400. The X-ray diffraction (XRD) measurements were carried out using Siemens D500 Goniometer. AVATAR 370 FT-IR from Thermo Nicolet was used for the FT-IR studies. Thermogravimetric analysis (TGA) of the hybrid materials were conducted in pure N_2 gas at a heating rate of 20 °C per min on a SDT Q 600 instrument. The electrochemical measurements were performed with an EG&G 273 potentiostat connected to a computer for data acquisition. A three-compartment electrochemical cell was used. The side arms contained a reference electrode and a platinum counter electrode. The hybrid materials were characterized on a glassy carbon electrode 1 mm in diameter polished with 6, 3 and 1 μm diamond then abundantly rinsed with ultrapure water, acetone and oven dried.

3. Results and discussion

3.1. Synthesis and physical properties of the hybrid materials

In this work, we have paired the well-Dawson anions $[H_4PW_{18}O_{62}]^{7-}$ and $[P_2W_{18}O_{62}]^{6-}$ with the organic 1-butyl-3-methylimidazolium cation $[BMIM]^+$, leading to the formation of organic–inorganic hybrid molecular solids. K, P, W and CHN elemental analysis of the powders showed that one mole of the Dawson dissymmetrical-type $[H_4PW_{18}O_{62}]^{7-}$ reacts with 6 moles of $BMIM^+$ cations, and one mole of the Dawson symmetrical-type $[P_2W_{18}O_{62}]^{6-}$ reacts with 4 moles of $BMIM^+$, to form, respectively, $K[BMIM]_6H_4PW_{18}O_{62}$ and $K_2[BMIM]_4P_2W_{18}O_{62}$ hybrid materials following the equations:

$$11\ [BMIM]BF_4 + K_7[H_4PW_{18}O_{62}] \rightarrow K[BMIM]_6H_4PW_{18}O_{62} + 5\ [BMIM]BF_4 + 6KBF_4 \quad (1)$$

and

$$6\ [BMIM]BF_4 + K_6[P_2W_{18}O_{40}] \rightarrow K_2[BMIM]_4P_2W_{18}O_{62} + 2\ [BMIM]BF_4 + 4KBF_4 \quad (2)$$

It is worth noting that not all the K^+ and protons cations were replaced by $BMIM^+$ cation during the synthesis, as expected initially.

Fig. 2 displays the morphology of the synthesized hybrid materials $K[BMIM]_6H_4PW_{18}O_{62}$ and $K_2[BMIM]_4P_2W_{18}O_{62}$. The SEM topography of the powder $K[BMIM]_6H_4PW_{18}O_{62}$ reveals clusters of irregular shapes and forms. By comparison, $K_2[BMIM]_4P_2W_{18}O_{62}$ displays more or less a homogenous morphology with various sized spherical nanoparticles. This difference in morphology might be related particularly to the number of the $BMIM^+$ present in each hybrid molecular material.

Fig. 3 shows a comparison between the powder X-ray diffraction (XRD) pattern of pure hydrated PW_{18} (Fig. 3a) and $K[BMIM]_6H_4PW_{18}O_{62}$ hybrid material (Fig. 3b), P_2W_{18} (Fig. 3c) and the corresponding hybrid material $K_2[BMIM]_4P_2W_{18}O_{62}$ (Fig. 3d). The well-Dawson PW_{18} and P_2W_{18} undergo structural transformation where, respectively, 6 and 4 protons and most of the H_2O molecules are replaced by $[BMIM]^+$ cations. The XRD pattern of the hybrid materials $K[BMIM]_6H_4PW_{18}O_{62}$ and $K_2[BMIM]_4P_2W_{18}O_{62}$ reveals a different structure compared to pure Dawson salts. XRD pattern illustrates that pure Dawson salts have ordered and defined structure, while the structure of the hybrid materials seems to be amorphous. This is understandable because the Dawson secondary structure is modified by the $[BMIM]^+$, since most of the sandwiched water molecules interacting with Dawson polyanions by hydrogen bonding are lost [29]. Another factor which might be the reason for the amorphous structure of the hybrid materials is the size. Compared to proton

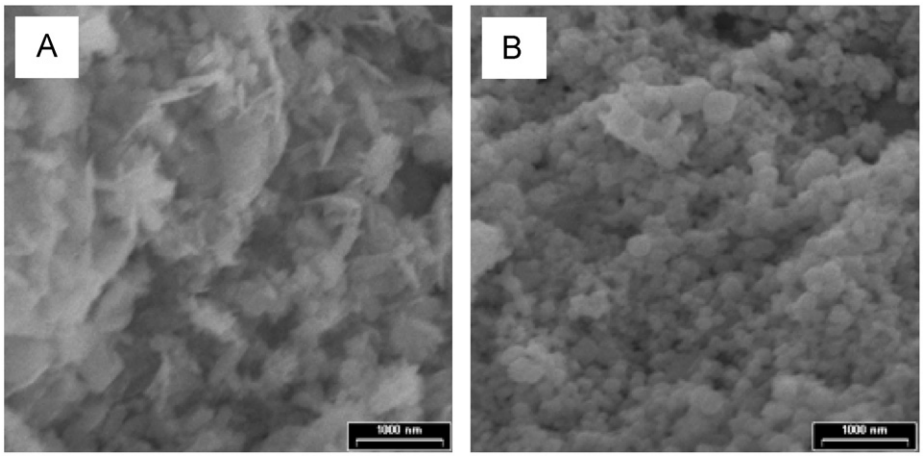

Fig. 2. SEM images of (A) $K[BMIM]_6H_4PW_{18}O_{62}$, and (B) $K_2[BMIM]_4P_2W_{18}O_{62}$.

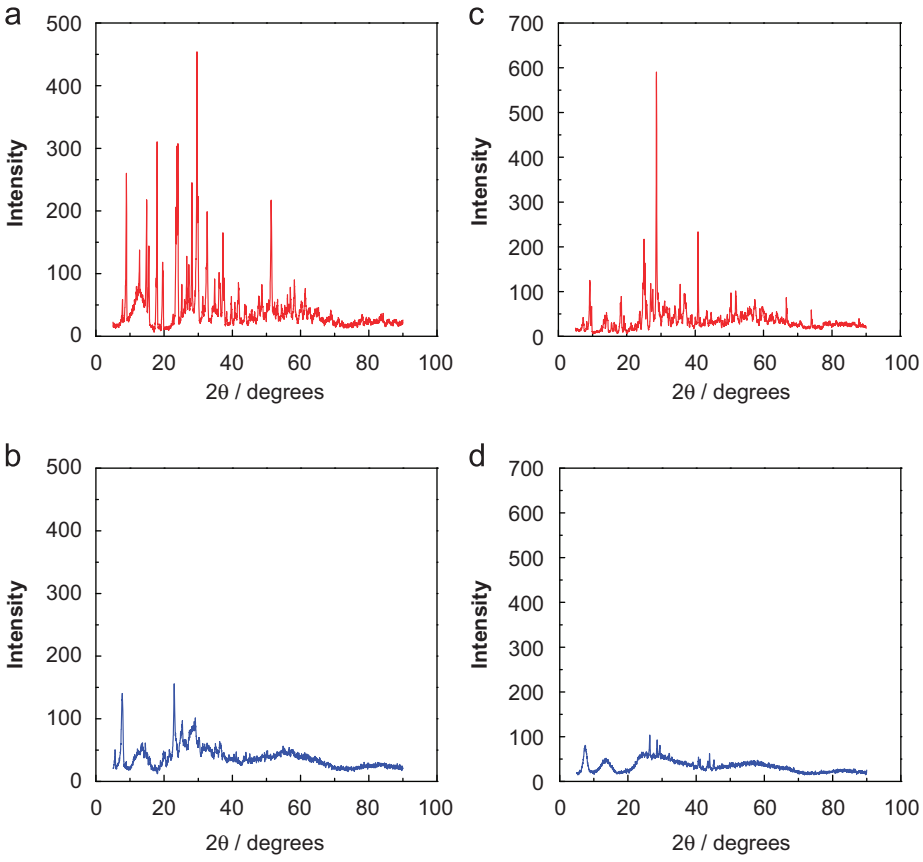

Fig. 3. Powder XRD pattern of (a) PW_{18}, (b) $K[BMIM]_6H_4PW_{18}O_{62}$, (c) P_2W_{18}, and (d) $K_2[BMIM]_4P_2W_{18}O_{62}$.

or water molecule, the size of $[BMIM]^+$ is quite large and this may screen out the Dawson structure in the hybrid material. This type of host–guest interactions are known to bring about structural transformations, which are detected by powder X-ray diffraction [30].

FT-IR spectra are useful to find out structural and bonding changes in the Dawson units in the hybrid materials. As can be seen from Fig. 4a, $[BMIM][BF_4]$ shows characteristic bands at 3149–2931 cm^{-1} (C–H str. in the imidazole ring), 1748 (imidazole –C═N– bending) [31], 1581–1464 cm^{-1} (imidazole ring str.), 1174–1027 cm^{-1} (imidazole H–C–C and H–C–N bending), 848 cm^{-1} (in-plane imidazole ring bending), 752 cm^{-1} (out of plane C–H bending of imidazole ring) and 657 cm^{-1} (imidazole C–N–C bending) [31]. The $[BMIM]^+$ can further be identified by spectral features in the regions of 700–550 cm^{-1}, 1800–1130 cm^{-1} and 3200–2800 cm^{-1} [32]. On the other hand, the parent PW_{18} Dawson structure shows characteristic bands at 3567–3287 cm^{-1} (H_2O), 1609 cm^{-1} (O–H bending), 1058–1035 cm^{-1} (P–O str.), 946 cm^{-1} ($W–O_{terminal}$ str.), 880 cm^{-1} (edge sharing W–O–W str.) and 707 cm^{-1} (corner sharing W–O–W str.)(Fig. 4b). As can be seen from Fig. 4c, the prominent FT-IR features due to PW_{18} ion cluster in the hybrid material are clearly marked in the stretching region of 1030–731 cm^{-1}, indicating that the primary Dawson structure is preserved in the hybrid material. It can also be seen in Fig. 4c that

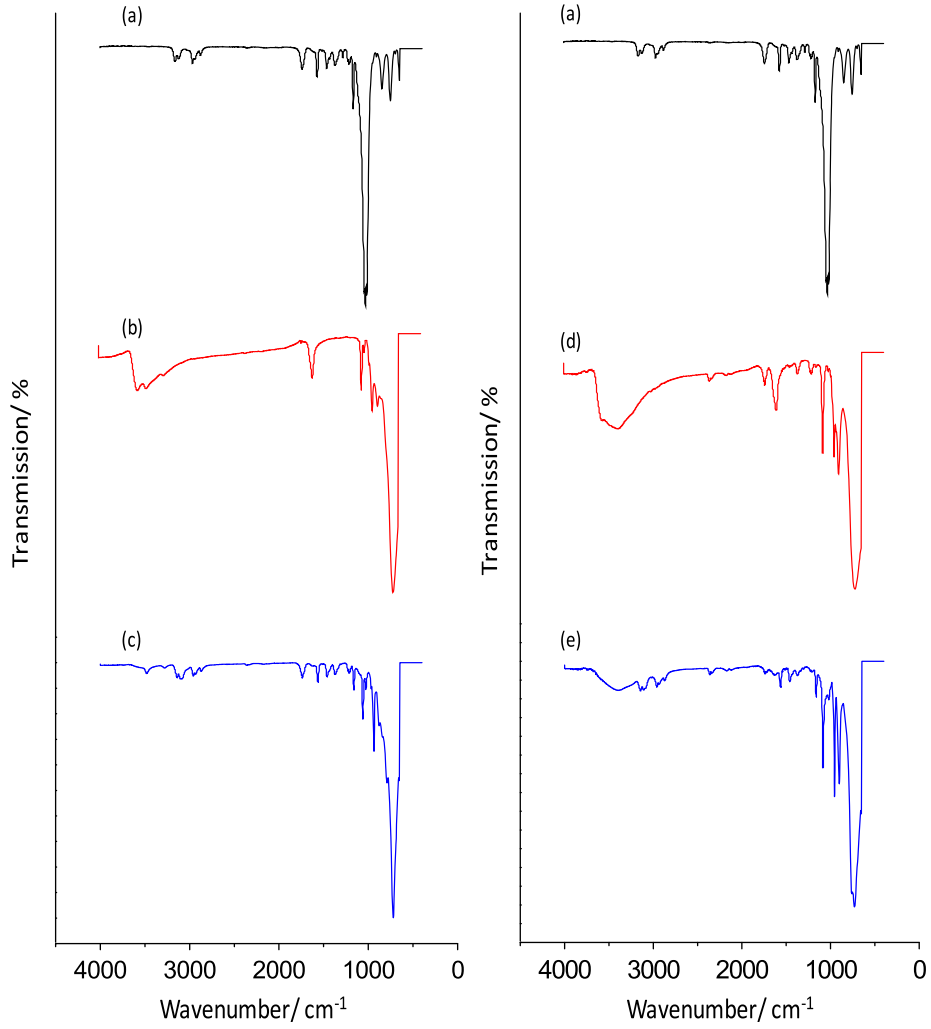

Fig. 4. FT-IR spectra of (a) $[BMIM][BF_4]$, (b) PW_{18}, (c) $K[BMIM]_6H_4PW_{18}O_{62}$, (d) P_2W_{18}, and (e) $K_2[BMIM]_4P_2W_{18}O_{62}$.

the water content (3567–3287 cm^{-1}) is significantly reduced in the hybrid material. More careful analysis of the spectra of Fig. 4c in the imidazolium ring C–H (3149–2931 cm^{-1}) and imidazolium ring C–H stretch (1581–1464 cm^{-1}) reveals that there is a strong electrostatic interaction between $[BMIM]^+$ cation and the Dawson PW_{18} anion. Similarly, FT-IR spectral data of the hybrid $K_2[BMIM]_4P_2W_{18}O_{62}$ and the parents $[BMIM][BF_4]$ and P_2W_{18} are shown, respectively, in Fig. 4e, a and d. The characteristic bands and their corresponding vibration mode are gathered in Table 1. Analysis of the FT-IR data shows that the basic structure and geometry of the Dawson anions entrapped in the $[BMIM]^+$ cations are preserved but the water content is reduced in the hybrid material.

The thermogravimetric behavior of $K[BMIM]_6H_4PW_{18}O_{62}$ hybrid molecular material and the parents $[BMIM][BF_4]$ and PW_{18} are shown in Fig. 5A. The TGA curve of $[BMIM][BF_4]$ shows a major weight loss at 400–600 °C, which reaches 100% at ~530 °C (Fig. 5Aa). This maybe attributed to decomposition of $[BMIM][BF_4]$ or eventually to its total evaporation. On the other hand, thermal analysis of PW_{18} illustrates a major weight loss at 70–350 °C and a minor loss at 350–600 °C (Fig. 5Ab). The first change in mass would be related to water loss, since PW_{18} contains constitution water molecules. The second minor loss is due to decomposition of the Dawson anion. These data are corroborated by differential scanning calorimetry, two main endotherms peaks are observed between 25 and 350 °C that are attributable to the loss of solvent water molecules and coordinated aqua ligands (Fig. 5Ab). As can be seen in Fig. 5Ac, the thermal stability of the hybrid material is quite improved compared to the parents $[BMIM][BF_4]$ and PW_{18}. Below 350 °C, no significant loss in weight can be observed, demonstrating that the water content in the hybrid material is reduced. Above 350 °C, significant weight loss is observed, which is estimated to be 22% at 600 °C. The latter will be ascribed to decomposition of both organic part and the inorganic Dawson anions in the hybrid molecular material. This is reflected in differential scanning calorimetry results, which illustrates a significant endotherm peak between 370 and 550 °C (Fig. 5Ac). Fig. 5B displays FT-IR spectra of $K[BMIM]_6H_4PW_{18}O_{62}$ thermally treated at different temperatures. It will be noted that no difference can be observed between the spectra of $K[BMIM]_6H_4PW_{18}O_{62}$ and $K[BMIM]_6H_4PW_{18}O_{62}$ heat treated at 200 °C, demonstrating the thermal stability of the hybrid material in this range of temperatures. In contrast, the spectra of $K[BMIM]_6H_4PW_{18}O_{62}$ heat treated at 450–600 °C are very different from the spectra of $K[BMIM]_6H_4PW_{18}O_{62}$ and show strong similarities with the spectra of $NaWO_4$ (Fig. 5Be). This demonstrates that at high temperatures the Dawson structure collapse forming WO_4 phase. By comparison, it is observed that the weight loss of the hybrid material $K_2[BMIM]_4P_2W_{18}O_{62}$ starts below 350 °C (data not shown), and the decrease in weights are more important than those recorded for $K[BMIM]_6H_4PW_{18}O_{62}$. For example, 23% and 41% are the weight losses registered at 300 and 600 °C, respectively.

Table 1
FT-IR bands of [BMIM][BF_4], P_2W_{18} and K_2[BMIM]$_4P_2W_{18}O_{62}$.

Wavenumbers (cm^{-1})			Vibration mode
[BMIM][BF_4]	**$K_6P_2W_{18}O_{62}.13H_2O$**	**K_2[BMIM]$_4P_2W_{18}O_{62}$**	
–	3395	3395	Water content
3149, 2931	–	3122, 2950	Imidazole ring (C–H str.)
1748	1736, 1609	1736	Imidazole –C=N- and/or O–H bending
1581, 1464	–	1569, 1459	Imidazole ring str.
–	1376, 1213	–	O–H bending
1174	–	1169	Imidazole H–C–C and H–C–N bending
1027	–	–	BF_4 anions
	1082	1091	P–O str.
–	957	952	W–O str.
–	909	902	Edge sharing W–O–W str.
848	–	–	In-plane imidazole ring bending
–	724	763	Corner sharing W–O–W str.
752	–	736	Out of plane imidazole C–H bending
657	–	660	Imidazole C–N–C bending

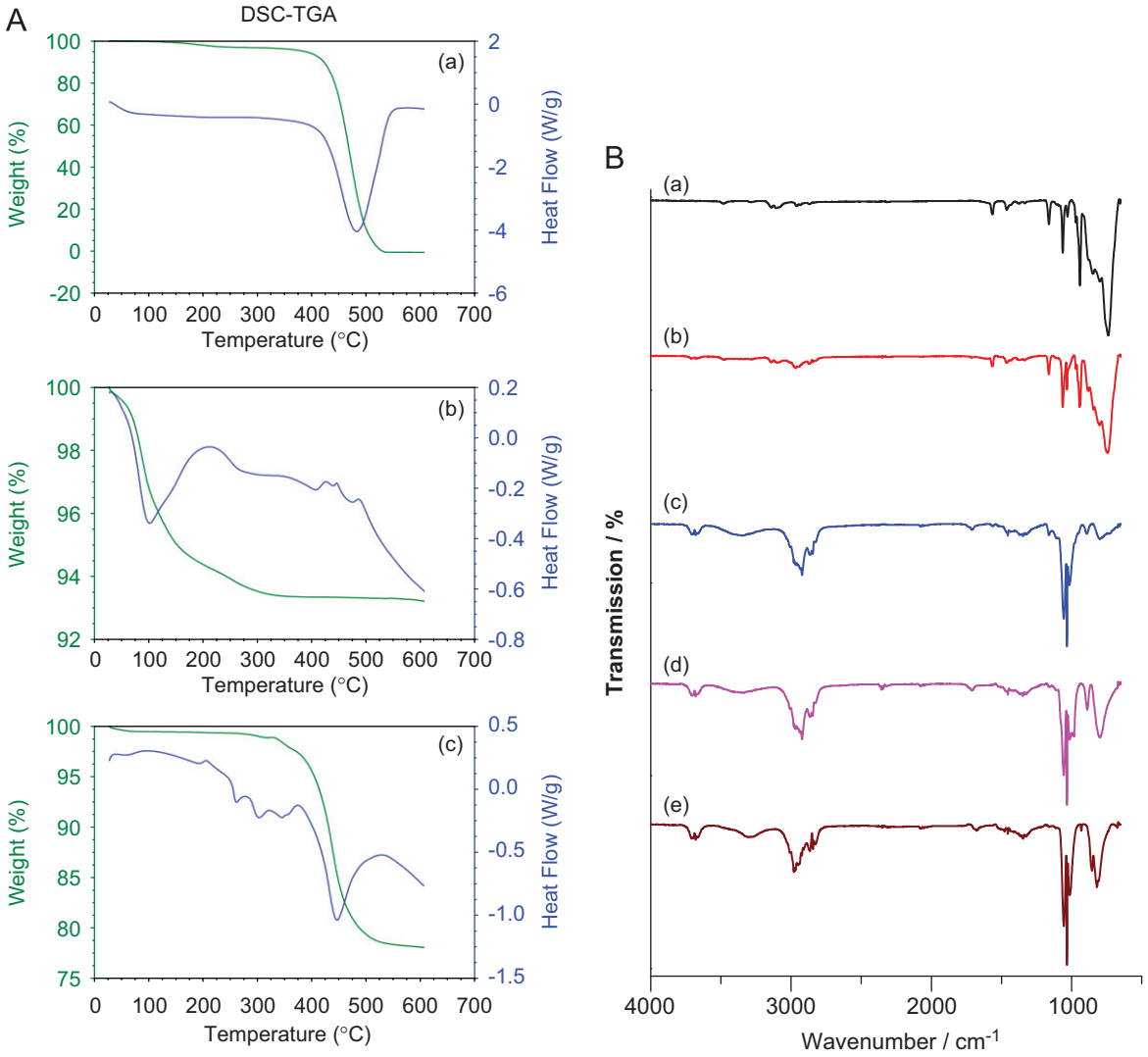

Fig. 5. (A) TG analysis of (a) [BMIM][BF_4], (b) PW_{18}, and (c) K[BMIM]$_6H_4PW_{18}O_{62}$ hybrid material. (B) FT-IR of K[BMIM]$_6H_4PW_{18}O_{62}$ thermally treated at room temperature (a), 200 °C (b), 450 °C (c), 600 °C (d) and, FT-IR of $NaWO_4$ (e).

3.2. Electrochemical studies

In order to better characterize the hybrid materials, cyclic voltammetry was used to study 1-butyl-3-methylimidazolium tetrafluoroborate, wells-Dawson POMs and the resulting hybrid materials. The cyclic voltammetry studies are carried out in dimethylsulfoxide (DMSO) as the hybrid materials are insoluble in water and in some organic solvents such as acetonitrile, ethanol and dimethylformamide. Fig. 6 (left) shows a comparison between the cyclic voltammograms of [BMIM][BF_4] (Fig. 6a), PW_{18} (Fig. 6b) and

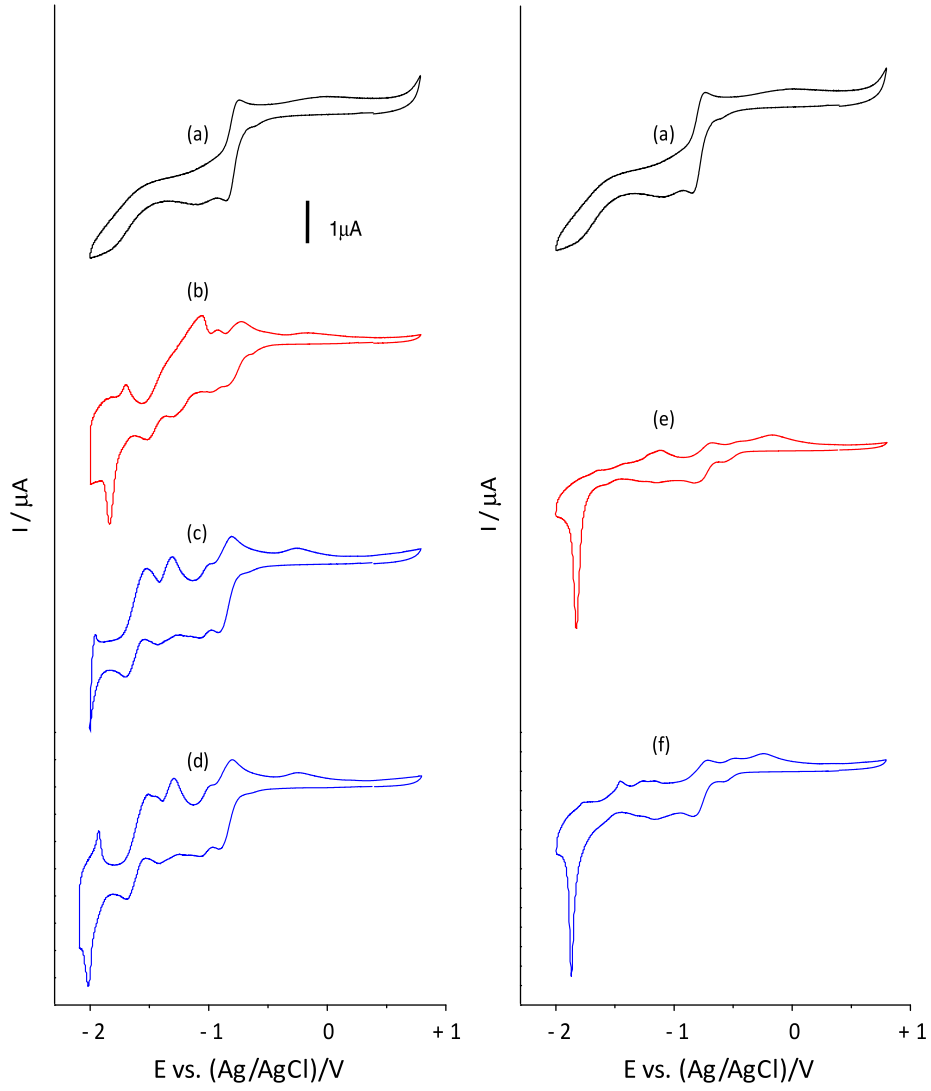

Fig. 6. Cyclic voltammetry curves of (a) $[BMIM][BF_4]$, (b) PW_{18}, (c and d) $K[BMIM]_6H_4PW_{18}O_{62}$, (e) P_2W_{18}, and (f) $K_2[BMIM]_4P_2W_{18}O_{62}$. Electrolyte: DMSO containing 0.1 M $NaClO_4$. Concentration: $\sim 5 \times 10^{-4}$ M. Scan rate: 20 mV/s. Reference electrode: Ag/AgCl.

the resulting hybrid material $K[BMIM]_6H_4PW_{18}O_{62}$ (Fig. 6c and d) in DMSO in presence of 0.1 M $NaClO_4$ as a supporting electrolyte. In the potential range from +0.8 to −2 V vs. Ag/AgCl, $[BMIM][BF_4]$ displays three reduction waves located, respectively, at −0.83, −1.08 and −1.84 V. No further redox waves have been observed at more positive or negative potentials. Corresponding to these reduction waves, two oxidation waves develop with their peak potentials located at −0.73 and +0.28 V. These waves might be attributed to reductions and oxidations within the imidazolium ring. As shown in Fig. 6b, PW_{18} displays five main reduction waves located at −0.82, 10.96, −1.29, −1.52 and −1.83 V. The last wave is a high intensity wave. These waves are attributed to reduction of the tungsten (W^{VI}) centers within PW_{18}. Corresponding to these reduction waves, four main oxidation waves can be distinguished with their oxidation peaks located respectively at −0.72, −0.90, −1.05 and −1.69 V. As displayed in Figs. 6c and d, the cyclic voltammogram of the hybrid material shows more or less the same shape and number of redox waves as PW_{18}. The most obvious difference is that the reduction waves of the hybrid material are shifted to negative potentials. For example, 0.08, 0.11, 0.12, 0.19 and 0.21 V are the shifts in potential observed for the five reduction waves of PW_{18} in the hybrid material. These shifts are quite significant and might be due to a decrease in the acidity of PW_{18} in $K[BMIM]_6H_4PW_{18}O_{62}$. In fact, six protons in PW_{18} have been replaced by six $[BMIM]^+$ in the hybrid material. In regard to the redox waves of the imidazolium cations $[BMIM]^+$ in the hybrid material, it is not clear from Fig. 6c and d whether they are present or not. Since the reduction waves of the imidazolium cation (Fig. 6a) lie almost at the same potentials as some of the reduction waves of PW_{18}, consequently, in the hybrid material the redox waves of imidazolium cations probably, merge with the redox waves of PW_{18}. On the other hand, the main reduction waves of the parent P_2W_{18} shown in Fig. 6e can easily be distinguished in the cyclic voltammogram of the hybrid material $K_2[BMIM]_4P_2W_{18}O_{62}$ (Fig. 6f). Compared to $K[BMIM]_6H_4PW_{18}O_{62}$, it can be seen that the peak potentials of the hybrid material $K_2[BMIM]_4P_2W_{18}O_{62}$ lie almost at the same values as the parent P_2W_{18}, except for the last reduction wave, which display a slight shift of 0.05 V towards negative values. This suggests practically no decrease in acidity of $K_2[BMIM]_4P_2W_{18}O_{62}$ compared to the parent P_2W_{18}. This was expected since $K[BMIM]_6H_4PW_{18}O_{62}$ contains 6 $[BMIM]^+$ cations and $K_2[BMIM]_4P_2W_{18}O_{62}$ contains only 4 $[BMIM]^+$. On the other hand, it is also possible to suggest from these results that the change in pKa (the acidity constant) of PW_{18} in the hybrid material is more significant than P_2W_{18} in the hybrid material. This difference was originally noticed for PW_{18} and P_2W_{18} [33]. The peak potentials of the reduction waves of the parents

Table 2
Peak potentials of the reduction waves of [BMIM][BF_4], P_2W_{18} and $K_2[BMIM]_4P_2W_{18}O_{62}$ hybrid material. Electrolyte: DMSO containing 0.1 M $NaClO_4$. Concentration: $\sim 5 \times 10^{-4}$ M. Scan rate: 20 mV/s. Reference electrode: Ag/AgCl.

Reduction waves/V vs. Ag/AgCl			Attribution
[BMIM][BF_4]	$K_6P_2W_{18}O_{62}.13H_2O$	$K_2[BMIM]_4P_2W_{18}O_{62}$	
–	−0.56	−0.56	Reduction of W^{VI} centers
−0.83	−0.80	−0.82	Reductions within imidazole rings + Reduction of W^{VI} centers
−1.08	−1.13	−1.14	Reductions within imidazole rings + Reduction of W^{VI} centers
−1.84	−1.82	−1.87	Reductions within imidazole rings + Reduction of W^{VI} centers

1-butyl-3-methylimidazolium tetrafluoroborate, P_2W_{18} and the hybrid material $K_2[BMIM]_4P_2W_{18}O_{62}$ are gathered in Table 2.

4. Conclusions

$K[BMIM]_6H_4PW_{18}O_{62}$ and $K_2[BMIM]_4P_2W_{18}O_{62}$ formed by reaction between 1-butyl-3-methylimidazolium tetrafluoroborate ionic liquid and $K_7[H_4PW_{18}O_{62}] \cdot 18H_2O$ or $K_6[P_2W_{18}O_{62}] \cdot 13H_2O$ have been investigated. XRD showed amorphous structure of the synthesized hybrid materials. FT-IR spectra showed the presence of both 1-butyl-3-methylimidazolium cations and the well-Dawson anions, but the water content decreased. TG analysis illustrated that compared to the parent reagents; the hybrid materials have relatively an improved thermal stability. Cyclic voltammetry in DMSO displayed that the reduction peak potentials of the Dawson anions in the hybrid materials shift towards negative potentials and the shift is more pronounced for $K[BMIM]_6H_4PW_{18}O_{62}$ than $K_2[BMIM]_4P_2W_{18}O_{62}$. This was related to a decrease in acidity of $[H_4PW_{18}O_{62}]^{-7}$ or $[P_2W_{18}O_{62}]^{-6}$ anions in the hybrid materials compared to the Dawson POMs. Future work will focused on using these hybrid materials for supercapacitor applications.

Acknowledgments

The authors acknowledge the support of the Research Fund KU Leuven (GOA/08/007) and the Belgian Federal Science Policy Office (BELSPO) through the IUAP project INANOMAT (contract P6/17). We thank Dimitri Soccol for the XRD data, Dirk Henot (Department of Chemistry KU Leuven) for the CHN elemental analyses, Danny Winant for TG analyses, Andrew Pedersen (UOIT) for the SEM images and Michael Allison (UOIT) for assistance with the ICP measurements.

References

[1] M.T. Pope, Heteropoly and Isopoly Oxometalates, Springer–Verlag, Berlin, 1983.
[2] B. Keita, L. Nadjo, J. Mol. Catal. A: Chem. 262 (2007) 190.
[3] C.L. Hill, in: A.G. Wedd (Ed.), Comprehensive Coordination Chemistry II: Transition Metal Groups 3–6, Elsevier Science, New York, 2004, p. 679.
[4] R. Content, G. Herve, Rev. Inorg. Chem. 22 (2002) 63.
[5] J.S. Anderson, Nature 140 (1937) 850.
[6] L.C. Baker, D.C. Glick, Chem. Rev. 98 (1998) 3.
[7] H.T. Evens Jr., J. Am. Chem. Soc. 70 (1948) 1291.
[8] U.L. Stangar, N. Groselj, B. Orel, Ph. Colomban, Chem. Mater. 12 (2000) 3745.
[9] C. Sanchez, G.J. de, A.A. Soler-Illia, F. Ribot, T. Lalot, C.R. Mayer, V. Cabuil, Chem. Mater. 13 (2001) 3061.
[10] J.A.F. Gamelas, A.M.V. Cavaleiro, E. De, M. Gomes, M. Belsley, E. Herdtweck, Polyhedron 21 (2002) 2537.
[11] L. Yang, H. Naruke, T. Yamase, Inorg. Chem. Commun. 6 (2003) 1020.
[12] M. Vasylyev, R. Popovitz-Biro, L.J.W. Shimon, R. Neumann, J. Mol. Struct. 656 (2003) 27.
[13] P. Gómez-Romero, K. Cuentas-Gallegos, M. Lira-Cantu, N. Casan-Pastor, J. Mater. Sci. 40 (2005) 1423.
[14] M. Vazylyev, D. Sloboda-Rozner, A. Haimov, G. Maayan, R. Neumann, Top. Catal. 34 (2005) 93.
[15] Y. Leng, J. Wang, D. Zhu, X. Ren, H. Ge, L. Shen, Angew. Chem. 121 (2009) 174.
[16] T. He, J. Yao, Prog. Mater. Sci. 51 (2006) 810.
[17] Y. Huang, Q.Y. Pan, X.W. Dong, Z.X. Cheng, Mater. Chem. Phys. 97 (2006) 431.
[18] U.L. Stangar, N. Groselj, B. Orel, A. Schmitz, Ph. Colomban, Solid State Ionics 145 (2001) 109.
[19] T. Rajkumar, G.Ranga Rao, Mater. Chem. Phys. 112 (2008) 853.
[20] G. Ranga Rao, T. Rajkumar, Babu Varghese, Solid State Sci. 11 (2009) 36.
[21] U.B. Mioc, M.R. Todorovic, M. Davidovic, Ph. Colomban, I. Holclajtner-Antunovic, Solid State Ionics 176 (2005) 3005.
[22] Z. Li, Q. Zhang, H. Liu, P. He, X. Xu, J. Li, J. Power Sources 158 (2006) 103.
[23] J.D. Kim, S. Hayashi, T. Mori, I. Honma, Electrochim. Acta 53 (2007) 963.
[24] P.G. Rickert, M.R. Antonio, M.A. Firestone, K. Kubatko, T. Szreder, J.F. Wishart, M.L. Dietz, Dalton Trans. (2007) 529.
[25] S. Liu, Z. Tang, Z. Wang, Z. Peng, E. Wang, S. Dong, J. Mater. Chem. 10 (2000) 2727.
[26] M. Ammam, J. Fransaer, J. Electrochem. Soc. 158 (2011) A14.
[27] R. Contant, S. Piro-Sellem, J. Canny, R. Thouvenot, C.R. Acad., Paris, Serie IIc, Chimie: Chem. Sci. 3 (2000) 157.
[28] R. Contant, Inorg. Synth. 27 (1990) 107.
[29] M. Misono, Chem. Commun. (2001) 1141.
[30] E. Choi, K. Park, C. Yang, H. Kim, J. Son, S.W. Lee, Y.H. Lee, D. Min, Y. Kwon, Chem. Eur. J 10 (2004) 5535.
[31] J. Coates, in: R.A. Meyers (Ed.), Interpretation of Infrared Spectra, A Pratical Approach, Encyclopedia of Analytical Chemistry, John Wiley&Sons Ltd, Chichester, 2000, pp. 10815–10837.
[32] W. Wu, W. Li, B. Han, Z. Zhang, T. Jiang, Z. Liu, Green Chem. 7 (2005) 701.
[33] I.M. Mbomekalle, B. Keita, Y.W. Lu, L. Nadjo, R. Contant, N. Belai, M.T. Pope, Eur. J. Inorg. Chem. (2004) 276.